Disorder-induced short-range ferromagnetism and cluster spin-glass state in sol-gel derived $La_{0.7}Ca_{0.3}Mn_{1-x}Cd_xO_3(0 \leqslant x \leqslant 0.2)$

Shilpi Karmakar, S. Taran, and B. K. Chaudhuri*
Department of Solid State Physics, Indian Association for the Cultivation of Science, Kolkata-700032, India

H. Sakata
Department of Applied Chemistry, Tokai University, 1117, Kitakaname, Hiratsuka, Kanagawa 259-1292, Japan

C. P. Sun, C. L. Huang, and H. D. Yang
Department of Physics, National Sun Yat-Sen University, Kaohsiung 804, Taiwan
(Received 17 January 2006; revised manuscript received 5 June 2006; published 7 September 2006)

Low temperature magnetic and transport properties of the sol-gel derived Cd doped $La_{0.7}Ca_{0.3}Mn_{1-x}Cd_xO_3(0 \leqslant x \leqslant 0.20)$ manganite system show ferromagnetism and cluster spin-glass behavior. Metal-insulator transition (MIT) is exhibited only by the samples with $x \leqslant 0.1$; and for higher concentrations ($x=0.15$ and 0.20), samples are semiconductors. The MIT shifts to the lower temperature regime with increasing Cd content, indicating an increase of disorder in the system. Structural analysis shows local strain-induced small lattice distortion of the MnO_6 octahedra with Cd doping. With increasing Cd content, the system undergoes interesting paramagnetic to ferromagnetic (with $x<0.10$) as well as paramagnetic to cluster spin-glass (for $x \geqslant 0.10$) transitions. ac susceptibility (χ_{ac}) and magnetic relaxation measurements confirm this cluster spin-glass behavior. χ_{ac} is found to follow the critical slowing down law ($\tau/\tau_0=\varepsilon^{-z\nu}$). The magnetic hysteresis loops indicate a field-induced irreversible ferromagnetic phase due to the presence of "weak" antiferromagnetic domains in the samples with $x \geqslant 0.10$. This typical behavior is found to be most prominent in the sample with $x=0.15$. The observed cluster spin-glass state is explained by considering the interactions between the ferromagnetic and antiferromagnetic clusters in these doped systems having disorder and reduced geometrical tolerance factor t, which resulted from the random substitution of Mn with Cd ions.

DOI: 10.1103/PhysRevB.74.104407 PACS number(s): 75.47.Lx, 71.30.+h, 75.47.Gk, 75.50.Lk

I. INTRODUCTION

Interesting properties such as colossal magnetoresistance (CMR),[1] charge/orbital ordering,[2] cluster/spin-glass ordering,[3] etc., shown by rare earth manganites $R_{1-x}A_xMnO_3$ (R=La, Pr, Nd, Sm, etc.; A=Ca, Sr, Ba, etc.) have attracted considerable attention in recent years. Though the parent compound $RMnO_3$ is an antiferromagnetic (AFM) insulator due to superexchange (SE) interaction between the Mn ions,[4] A-site doped compound ($\sim 0.2<x<0.4$) is ferromagnetic (FM) and usually metallic below the metal-insulator transition (MIT) temperature T_P. Such property is explained on the basis of Zener double-exchange (DE) mechanism.[5] In addition to SE and DE interactions, lattice distortion also plays a dominant role through strong electron-lattice coupling or polaronic effect, which arises from the Jahn-Teller effect around the Mn^{3+} ions.[6] Strength of FM and AFM interactions and competition between them determines the observed magnetic and transport properties of the manganite system. Recently, in the mixed valent system, an important role of intrinsic disorder was recognized concerning the inhomogeneous state found on various scales from the formation of polaronic clusters or cluster magnetic regions upto a large-scale phase separation. The Mn-O network plays an important role in understanding the transport and magnetic behavior of these materials, and substitution at Mn site promotes intrinsic disorder in the system modifying the properties of these manganites. The nature (ionic size, valence state, etc.) of the element substituting the Mn site is also a very important factor modifying the properties of the resultant compound. For example, Co substitution in $La_{0.7}Ca_{0.3}MnO_3$ and $La_{0.7}Pb_{0.3}MnO_3$ leads to cluster-glass ferromagnetic ordering from the usual long-range order.[7] Similarly, Fe doping in $La_{0.7}Pb_{0.3}MnO_3$ leads to localization of electronic carriers and subsequent frustration of long range magnetic order.[8] Cr^{3+} doping in $La_{0.67}Sr_{0.33}MnO_3$ effects the magnetoresistance by introducing DE between Cr and Mn,[9] whereas in $La_{0.7}Ca_{0.3}MnO_3$, Cr doping at Mn site induces spin-cluster effect.[10]

It is also worth noting that doping with nonmagnetic $3d^0$ or $3d^{10}$ ions at Mn site gives a chance to study the lattice effects without introducing any extra magnetic background. Substitution of Mn by Mg^{2+}, Zn^{2+}, Al^{3+}, etc., in a charge order (CO) system introduces random disorder and destroys the charge ordering,[11,12] whereas in a FM manganite system, a decrease in ferromagnetic volume and FM-to-PM (paramagnetic) transition temperature T_C is observed.[13,14] Fan *et al.*[13] studied the effect of Mg^{2+} doping at Mn site of the $La_{0.67}Sr_{0.33}MnO_3$ system and observed cluster/spin-glass state. The appearance of such glassy or cluster phase is emphasized in several other reports on Mn site doped manganite systems.[15,16] For the A-site doped systems, size of the impurity ion in the A-site is a crucial factor determining the spin-glass state.[3] However, it is still not confirmed whether in the Mn site doped systems, spin-glass state depends on the tolerance factor t $[=(d_{A\text{-}O})/\sqrt{2}(d_{Mn\text{-}O})]$ similar to that of the A-site doped systems.[17]

Blasco *et al.*[18] concluded from their transport and magnetic studies that in spite of larger cationic size of the Mg^{2+}

ion compared to that of the Mn^{3+} ion in the $LaMnO_3$ system, the Mg^{2+} ion substitutes only for the Mn^{3+} ion and not the larger sites of La^{3+} ion. Substitution of Mn with Cd^{2+}, having a larger ionic size, appears to show interesting physical properties, not only because it is nonmagnetic, but it is also a good candidate for studying the disorder effects, local changes in the lattice constants, valency effects, and their relation with properties such as resistivity, spin freezing, etc. Moreover, the effect of a large Cd ion at the Mn site is studied only on a few charge ordered insulator (COI) manganites.[19] For understanding the effects of Cd doping on the FM manganite and CMR materials, in general, further investigation of Cd doped system over a wide concentration of Cd is important. In this paper, our plan is to elaborately study the effect of Cd doping on the transport and magnetic properties of well-characterized $La_{0.7}Ca_{0.3}Mn_{1-x}Cd_xO_3$ system over a wide range of Cd concentration ($x=0$, 0.01, 0.05, 0.10, 0.15, and 0.20). The system is found to show interesting cluster/spin-glass behavior, in a limited doping region.

Our organization of the manuscript is as follows. In Sec. II we discuss in brief the method of sample preparation by sol-gel technique and characterization of the samples using x-ray diffraction (XRD), x-ray photoelectron spectroscopy (XPS), scanning electron microscopy (SEM), superconducting quantum interference device (SQUID) magnetometer, etc. Section III deals with the experimental results and discussion on the transport and magnetic measurements, elucidating the cluster/spin-glass behavior and its probable origin. A comparison of our results with those of other similar interesting systems has also been made. The paper ends with a general conclusion on the transport and magnetic properties of the Cd doped $La_{0.7}Ca_{0.3}MnO_3$ system.

II. EXPERIMENT

All the polycrystalline samples $La_{0.7}Ca_{0.3}Mn_{1-x}Cd_xO_3$ ($x=0$, 0.01, 0.05, 0.10, 0.15, and 0.20) were prepared by sol-gel method.[20] The dried gels were calcined in air at 800 °C for 15 h, at 900 °C for 4 days, and at 1000 °C for 30 h with intermediate grindings. The resultant powder was pressed into pellets and sintered in air at 1000 °C for 24 h. X-ray diffraction studies were carried out on a Siefart Philips diffractometer to obtain structural information at room temperature. The x-ray photoelectron spectroscopy (XPS) was undertaken in Japan with monochromatic Al-K_α radiation (150 W) in a Kratos Axis spectrometer. Resistivity and magnetoresistance measurements were done using the standard four-probe method with connections made with silver paint. The dc and ac magnetic measurements were made on a SQUID and a MPMS measurement system (Quantum Design) in Taiwan from temperatures ranging from 5 K to 350 K.

III. RESULTS AND DISCUSSION

Figures 1(a) and 1(b) show SEM micrographs for typical samples with $x=0$ and 0.20, respectively. The grains exhibit homogeneity in size (<1 μm) and in crystallization. Figures 2(a) and 2(b) show the x-ray diffraction patterns along with

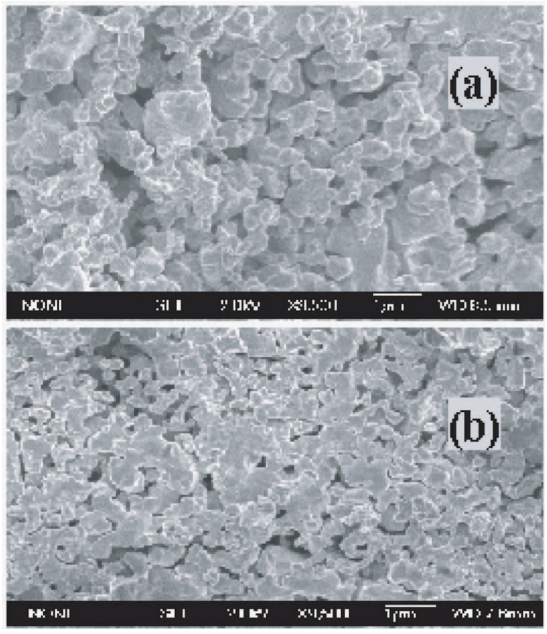

FIG. 1. (a) and (b) scanning electron micrographs (SEM) for samples with $x=0$ and $x=0.20$, respectively.

the fitted curves. Table I summarizes the relevant structural parameters obtained by Rietveld analysis of the diffractograms by using the FULLPROF program. Addition of Cd in the orthorhombic (*Pbnm*) $La_{0.7}Ca_{0.3}MnO_3$ system introduces a minor tetragonal (*I*4/*mcm*) phase in higher doped samples ($x \geqslant 0.15$). The refinement result indicates that the concentration of the tetragonal phase increases with increasing x, from 1.5% for $x=0.15(a=b=5.4384, c=7.7577)$ Å to 5.7% for $x=0.20(a=b=5.4011, c=7.7874)$ Å. Our XRD results are in agreement with the previous ones[21] where the orthorhombic and tetragonal phases were found to coexist. Woodward *et al.*[21] have suggested that the presence of the tetragonal phase prefers AFM *A* state. The unit cell volume of *I*4/*mcm* phase is smaller than that of *Pbnm*. The result suggests that Cd^{2+} doping in the $La_{0.7}Ca_{0.3}MnO_3$ system favors the tetragonal *I*4/*mcm* phase. Since the ionic radii of $Cd^{2+} > Mn^{3+} > Mn^{4+}$ ($0.95 > 0.645 > 0.53$) Å (Ref. 22), two factors are important in deciding the structure of the system. Increase of Cd^{2+} will increase the bond length and again since the charge equilibrium has to be preserved, Mn^{3+} (larger) will be oxidized to Mn^{4+} (smaller) and therefore the bond length will decrease. This competing situation leads to resultant changes in bond length and bond angle. From Table I, it is seen that the unit cell constants and cell volume V tend to increase with the addition of Cd. The average Mn-O-Mn bond angle becomes smaller and the Mn-O1 (O1=apical oxygen) bond tend to elongate with increasing Cd concentration. However, one of the Mn-O2 (O2=basal oxygen) bonds increases whereas the other one decreases in length. This indicates that the partial substitution of Mn by Cd of higher ionic radius gives rise to an additional dopant-size-induced local strain effect.

Although there is no tabulated ionic radius for a ninefold coordinated Cd^{2+} ion[22] with oxygen atoms, we are, however, not neglecting the possibility that Cd^{2+} is substituted at the perovskite *A* site for lower Cd doped samples or segregation

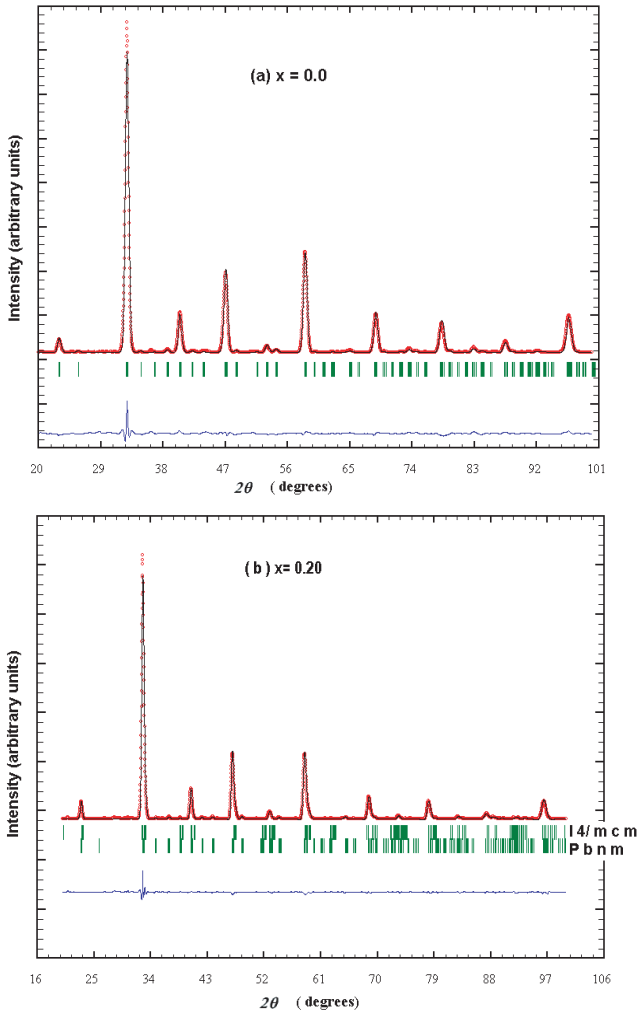

FIG. 2. (Color online) (a) and (b) x-ray diffraction patterns along with the fitted curves for the typical $La_{0.7}Ca_{0.3}Mn_{1-x}Cd_xO_3$ ($x=0$ and 0.20) samples.

of CdO for higher doped samples. It is also true that improper substitution of Cd would have resulted in extra nonperovskite phases. Since no such noticeable phases were observed, Cd^{2+} is considered to be substituted at the Mn site. This is confirmed from the XPS measurements performed for $x=0.0$ and $x=0.10$ samples. The quantitative analysis indicates proper cationic concentrations. In Figs. 3(a)–3(d), the La3*d*, Ca2*p*, Mn2*p*, and Cd3*d* core level spectra are shown. The core level binding energies are given in Table II. The increased value of Mn^{4+} concentration in the $x=0.10$ compared to that of the $x=0$ sample leads to the increase of the overall Mn valence and hence the binding energy (BE) peaks shifts (+0.15 eV) towards higher BE side. This result is consistent with the theoretically estimated value (=0.144 eV, since the chemical shift of the Mn2*p* edge in manganites is +1.0 eV/valence unit[23]).

A. Transport properties

Figure 4(a) demonstrates that resistivity of the sample increases with increasing Cd content. For $x \leqslant 0.10$, the samples show MIT at T_p. For $x>0.10$, the samples show semiconducting behavior over the entire measuring temperature range (80–300 K). The role of Cd in the decrease of T_P and in the increase of CMR could be understood in two ways.[24] The doping of Cd promotes the random character of the distribution of Mn-site ions (Mn^{3+}, Mn^{4+}) and Cd^{2+}, leading to the random distribution of hopping centers and exchange character between the localized spins. The presence of Cd^{2+} ions, unable to acquire higher valence, would induce a longer residence time of the higher valence of Mn^{4+} in its immediate neighborhood. Since Mn^{4+} is a smaller ion, the suggested local charge arrangement will release the strain on the system. Secondly, an increase in Cd content leads to the formation of clusters because there is no exchange interaction between Cd^{2+} and Mn ions. So the long-range ordering gradually reduces to short-range ordering in the clusters. The increase in resistivity [Fig. 3(a)] at low temperature also suggests the formation of such clusters.[25] The FM conducting cluster formation within the PM resistive regions also lowers the value of T_P. The cluster size in the phase separation region is governed by the strength of disorder: the smaller the disorder, the larger the cluster size. The resistivity does not decrease until the regions between magnetic clusters become thin enough that they are no longer a barrier to the conduction mechanism. Therefore, since the extent of disorder grows with Cd doping, one may expect that the cluster size will be reduced as x is increased in the small doping region. This means that the phase separation around T_P in $La_{0.7}Ca_{0.3}Mn_{1-x}Cd_xO_3$ is in the form of many small isolated metallic clusters (islands) coexisting with insulating areas. The competing antiferromagnetic superexchange couplings Mn^{3+}-O-Mn^{3+} and Mn^{4+}-O-Mn^{4+} may also distort the lattice and influence the cluster size in the phase separation region.

Near room temperature, the resistivity curves are more or less parallel, indicating that the activation energy of carriers is nearly independent of x in this region. The increase in the value of resistivity with x around room temperature is due to the reduction in carrier density with the increase in Cd doping and broadening the forbidden band near the Fermi level, thus blocking the electron transport. This can be observed by fitting the resistivity data with theoretical models. It is seen from Fig. 3(b) that the semiconducting region ($T>T_P$) of the resistivity curves of the present samples follow Mott's variable range hopping,[26] viz., $\rho=\rho_0 \exp(T_0/T)^{1/4}$. The fitting parameter T_0, summarized in Table III, is related to the localization length, L, by the relation $k_B T_0=18[L^3N(E)]$, where k_B is the Boltzmann constant, and $N(E)$ is the density of states. Since Cd doping directly effects the Mn^{3+}/Mn^{4+} ratio, it is reasonable that $N(E)$ will be dependent on the Cd content. In practice, however, L is also expected to be effected by Cd^{2+} doping, but for a constant L (~0.45 nm),[26] it is seen from Table III that $N(E)$ decreases sharply as Cd doping is increased.

The corresponding magnetoresistance of the samples {MR=$[\rho(0)-\rho(H)]/\rho(0)$, where $\rho(H)$ is the resistivity in applied field H (~1.15 T)} as a function of temperature is shown in Fig. 4(c). It is observed that with increasing Cd content, the MR ratio increases. Cd^{2+} substitution not only reduces the hole density but also enhances localization of

TABLE I. Some selected refined cell parameters obtained from x-ray diffraction analysis (Reitveld refinement) of the $La_{0.7}Ca_{0.3}Mn_{1-x}Cd_xO_3$ (x=0, 0.01, 0.10, 0.15, and 0.20) samples.

Parameter/x	x=0.0	x=0.01	x=0.10	x=0.15	x=0.20
a (Å)	5.4786	5.4877	5.5163	5.5088	5.5118
b (Å)	5.4663	5.4603	5.4685	5.4542	5.4545
c (Å)	7.7201	7.7285	7.7286	7.7108	7.7366
V (Å^3)	231.20	232.58	233.14	231.67	232.59
Mn-O1[a]	1.957	1.959	1.961	1.958	1.961
Mn-O2[a]	1.959	1.963	2.005	1.974	1.966
	1.955	1.955	1.942	1.956	1.953
⟨Mn-O⟩	1.9570	1.9590	1.9693	1.9626	1.9600
Mn-O1-Mn	161.1	159.2	158.9	160.2	160.6
Mn-O2-Mn	160.5	160.8	160.6	159.6	158.3
⟨Mn-O-Mn⟩	160.8	160.0	159.7	159.9	159.4
R_p (%)	8.8	7.5	7.1	7.6	9.5
R_{wp} (%)	11.1	10.6	10.4	10.8	12.5
χ^2	3.58	3.62	3.78	3.60	3.23

[a]O1=apical oxygen, O2=basal oxygen atom.

holes due to a random field. However, an external magnetic field might delocalize the holes. It has already been discussed that Cd substitution destroys long-range ordering and promotes short-range ordered cluster formation, the moments of these clusters arrange randomly and weaken the coupling between the FM spins of the clusters. Therefore, it is easier to align the moments of the clusters under an external applied field. This explains the observed increase of MR with increasing x.

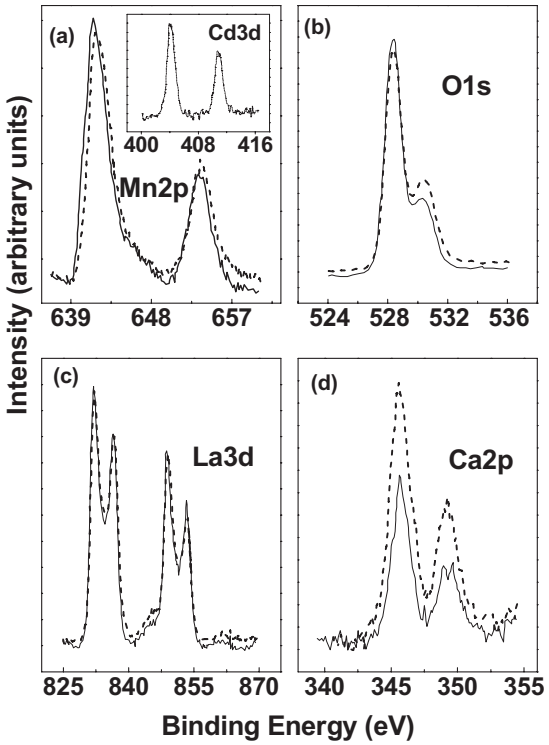

FIG. 3. (a)–(d) XPS spectra of the samples with x=0 (bold line) and 0.10 (dashed line). Core energy levels for (a) Mn2p (inset, Cd3d for x=0.10), (b) O1s, (c) La3d, and (d) Ca2p are shown.

B. Magnetism and spin glass behavior

Figures 5(a) and 5(b) represent the temperature dependent zero field cooled (ZFC) and field cooled (FC) magnetization (M) in 500 Oe magnetic field for the present samples. With increasing Cd content, the value of M decreases and the PM-FM transition temperature shift to lower temperatures. The Curie temperatures T_C, which is defined as the inflection point in the M-T curves, are summarized in Table III. The low temperature ZFC magnetization shows a drop with cooling, for the highly doped sample ($x \geqslant 0.10$). The steep drop of ZFC magnetization at low temperature signifies the formation of a cluster/spin-glass state. In fact, previous reports also indicated that a cluster/spin-glass behavior is broadly observed in Mn-site doped manganites.[7,10,13,27] Apart from frustration arising due to FM and AFM regions, the zero moment of Cd^{2+} ions also plays a key role in the magnetic behavior. To clarify it, we have measured M-H curves for the samples. Figure 6 shows the magnetization behavior of the present samples as a function of magnetic field (−6 T to +6 T) over all four quadrants at 5 K. For the samples, with x=0, 0.01, and 0.05, M rises sharply at low fields and tends to saturate at high fields. However, for the $x \geqslant 0.10$, the M-H behavior is quite different. After showing a steep rise in the low field range ($\mu_0 H < 0.5$ T), the magnetization still in-

TABLE II. XPS core-level binding energies (in eV) of $La_{0.7}Ca_{0.3}Mn_{1-x}Cd_xO_3$ samples with x=0 and 0.10.

x	La3$d_{5/2}$	Ca2$p_{3/2}$	Mn2$p_{3/2}$	O1s	Cd3$d_{5/2}$
0.0	833.6	346.5	641.50	529.3	NA
0.10	833.6	346.5	641.65	529.4	404.6

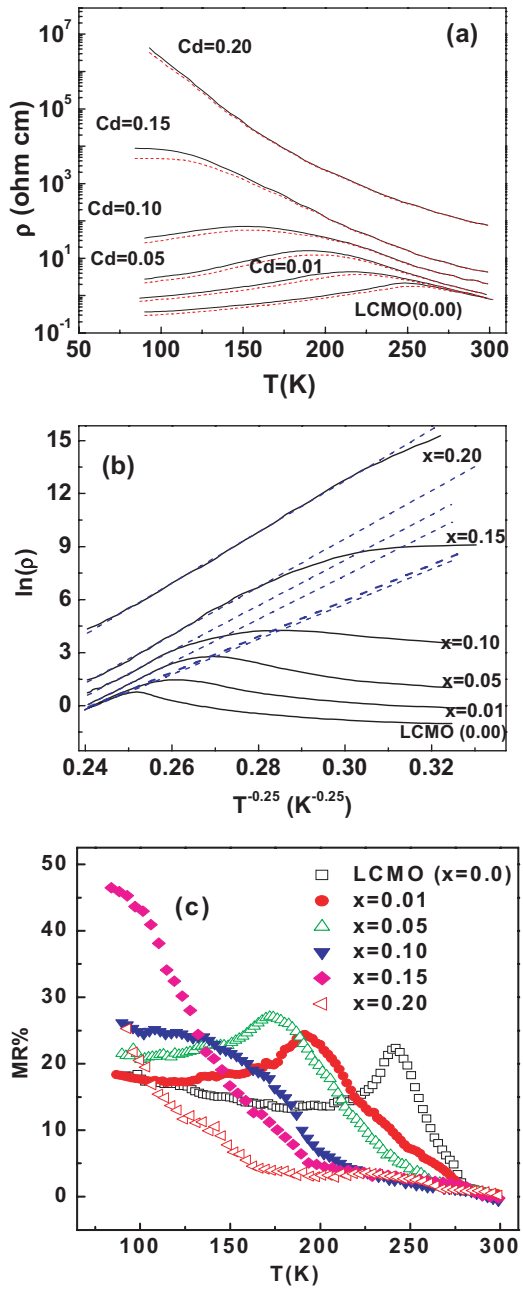

FIG. 4. (Color online) (a) Temperature dependence of the resistivity taken at $H=0$ T solid line and $H=1.15$ T dashed lines. (b) $\ln(\rho)$ vs $T^{1/4}$ T for the $La_{0.7}Ca_{0.3}Mn_{1-x}Cd_xO_3$ ($x=0$, 0.01, 0.05, 0.10, 0.15, and 0.20) samples. Solid lines represent experimental data and dashed lines are the best fit to the resistivity data above T_p according to the Mott's VRH model discussed in the text. (c) Temperature dependencies of MR $\{=[\rho(H=0)-\rho(H=1.15\ \text{T})]/\rho(H=0)\}$ for the series $La_{0.7}Ca_{0.3}Mn_{1-x}Cd_xO_3$ with $x=0$, 0.01, 0.05, 0.10, 0.15, and 0.20.

creases steadily with increasing magnetic field and does not show any sign of saturation, even at 6 T (at low temperature 10 K), which indicates the presence of glassy phase in the system. From Fig. 6 (insets) we see that the samples with $x=0.10$, 0.15, and 0.20 exhibit a peculiar field-induced effect at 5 K in the hysteresis loop. The numbers and arrows in the figures indicate the sequence and direction of field sweep. At 5 K with the application of field, M increases rapidly, showing a FM characteristic. Then M increases almost linearly with increasing field. In the down-sweep process, M stays at the high value until H decreases to zero, showing a loop in the first quadrant. In the third sweep process, in which H was applied in the opposite direction, the absolute value of M increases rapidly to the high value with the increase of $|H|$. As H goes back to zero in the fourth sweep, the M coincides with that of third sweep. Then the fifth sweep coincides with that of the second sweep instead of the first sweep. This field-induced FM state is also observed recently in a few other manganite systems showing competing magnetic phases[28–31] and can be explained by the presence "weak" AFM domains in the system.[29] When the applied field is small ($H<1$ T), these weak domains remain in their AFM state, while a relatively larger field ($H>1$ T) can destroy this AFM interaction and the spins can be flipped. As observed from Fig. 6, this field-induced effect is more prominent for the sample with $x=0.15$ than that observed with $x=0.10$ and 0.20. This is due to the fact that the number and strength of weak AFM domains are optimum for the sample with $x=0.15$. Whereas for $x=0.10$, the number of weak AFM domains is small, for $x=0.20$, the AFM interaction is strong enough to overcome the field-induced ferromagnetism. This also explains why this training effect was observed prominently only for one typical concentration in the spin-glass manganite, viz., $La_{0.7-x}Dy_xCa_{0.3}Mn$ (Fe)O_3 system, recently reported by Bhargava *et al.*[30]

In order to confirm the spin/cluster-glass behavior, low temperature ac susceptibility, χ_{ac} of the samples were also studied in details for $x=0.15$ and 0.20, they show maximum divergence in the ZFC and FC curves. In Figs. 7(a) and 7(b), we present the temperature variation of the real χ' (dispersion) and the imaginary part χ'' (absorption) of χ_{ac}, respectively, with temperature at different frequencies of the alternating field. The χ' curves exhibit clear peaks while the corresponding χ'' curves show inflection around the spin/cluster-glass transition temperature T_g. The height of the peak around T_g decreases slightly and is shifted to higher temperatures with increasing frequency f. The increase of T_g with frequency is a characteristic of the spin-glass state and is usually estimated from the quantity $k=\Delta T_g/T_g\Delta(\log_{10} f)$, where Δ refers to the difference. Knowing T_g from the maximum of the χ' curves or from the inflection of the χ'' curves, we obtain $k=2.1\times10^{-2}$ for $x=0.20$, which agrees with the values for typical spin-glass systems, e.g., 2.0×10^{-2}, 1.8×10^{-2}, and 6×10^{-2} for $La(Fe_{1-x}Mn_x)_{11.4}Si_{1.6}$, NiMn, and (EuSr)S, respectively.[32] The sharpness of the peak observed in χ is a sign of a homogeneous phase transition.[32] From Fig. 7(b) we see that the phase transition from a PM state to a spin-glass state is pronounced in the sample with $x=0.20$ whereas for the sample with $x=0.15$ this is relatively wider. From each susceptibility curve, one can define a frequency dependant freezing temperature T_f, below which the longest relaxation time of the system exceeds the observation time τ_{obs} (=1/f characteristic of the measurement) and the system is out of equilibrium. Figure 8(a) also shows scaling of $\tau(T_f)=t_{obs}$ with reduced temperature $\varepsilon=[(T_f-T_{SG})/T_{SG}]$. Using the conventional critical slowing power law relation

TABLE III. Some chemical, structural, transport, and magnetic parameters of $La_{0.7}Ca_{0.3}Mn_{1-x}Cd_xO_3$ ($0>x>0.20$) samples. The meaning of the terms is described in the text.

Parameter/x	$x=0.0$	$x=0.01$	$x=0.05$	$x=0.10$	$x=0.15$	$x=0.20$
Mn^{4+}	0.3	0.31	0.35	0.40	0.45	0.50
Mn^{3+}	0.7	0.68	0.60	0.50	0.40	0.30
t	0.922	0.921	0.917	0.913	0.908	0.904
$\rho_{300\ K}$ (ohm cm)	0.825	0.864	1.063	2.077	4.316	76.9
T_P (K)	248	217	189	155	[a]	[a]
$T_0\times10^8$ (K)	0.967	1.060	2.289	2.713	3.435	4.389
$N(E)\times10^{25}$ eV^{-1} cm^{-3}	2.369	2.161	1.013	0.8448	0.6672	0.5222
T_C or T_g (K)	240	172	148	43	45	40
M_S (μ_B)	3.63	3.56	3.25	2.99	2.78	2.14
M_S (Theoretical) (μ_B)	3.7	3.65	3.45	3.2	2.95	2.7

[a]No MIT.

($\tau/\tau_0=\varepsilon^{-z\nu}$), linear in a log-log scale, a good scaling is observed for $T_{SG}=42.1\pm0.5$ K, $\tau_0=10^{-12}$ s, and $z\nu=10.8\pm1.6$ for the sample with $x=0.20$. This means that the time necessary to reach equilibrium becomes longer and longer as the sample approaches $T_{SG}\sim42.1$ K, and the relaxation time diverges at T_{SG} as $\varepsilon^{-z\nu}$ (z and ν are critical exponents). τ_0 represents the microscopic flipping time of the fluctuating entities, which in the present case is close to that of microscopic spin-flip time ($\sim10^{-13}$ s). The value of $z\nu$ is similar to that of other manganite spin-glass systems and conventional spin glasses.[32] From Fig. 8(a) we also observe that although the glass transition temperature T_f for the $x=0.15$ sample is frequency dependent, it does not follow any linear relation. Thus we may note that the spin-glass state is not homoge-

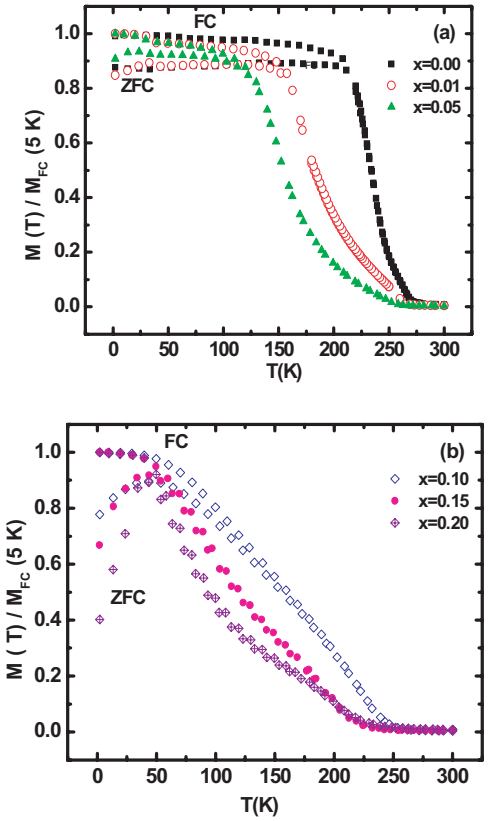

FIG. 5. (Color online) dc magnetization curves of $La_{0.7}Ca_{0.3}Mn_{1-x}Cd_xO_3$ with $x=0$, 0.01, 0.05, 0.10, 0.15, and 0.20 in an applied field of 0.05 T. The term $M(5\ K)$=field cooled magnetization at $T=5$ K.

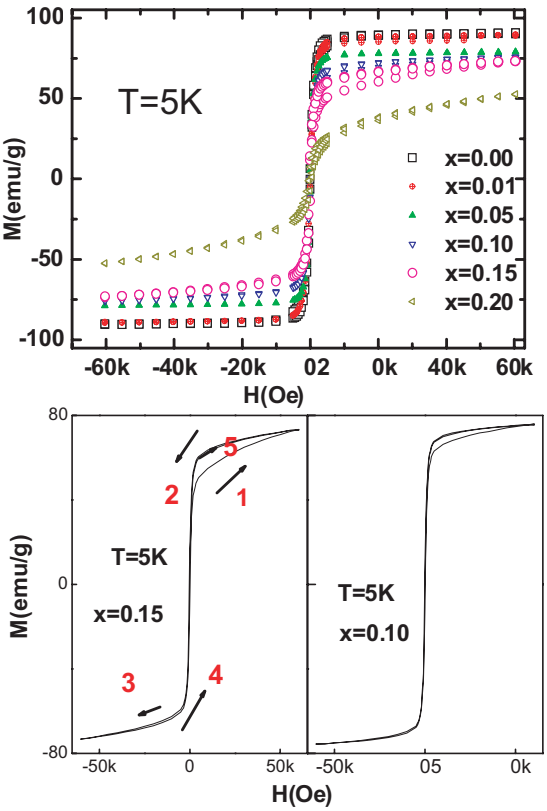

FIG. 6. (Color online) The magnetic hysteresis loops for the Cd doped samples in a magnetic field from −6 T to +6 T at 5 K. The numbers and arrows in the insets indicate the sequence and direction of the field sweep.

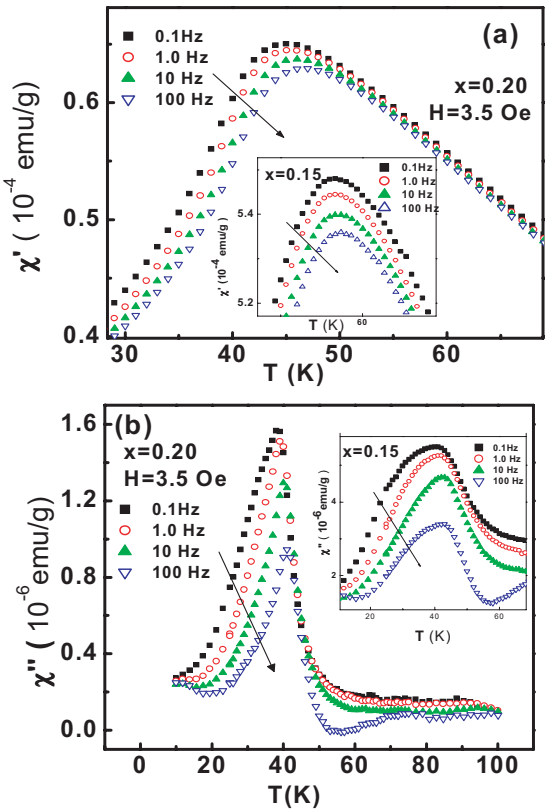

FIG. 7. (Color online) (a) The temperature dependence of the real (χ') and (b) imaginary (χ'') part of the ac susceptibility χ_{ac} under different frequencies from 0.1 to 100 Hz for the $La_{0.7}Ca_{0.3}Mn_{1-x}Cd_xO_3$ sample with $x=0.20$. The inset displays the corresponding parts of the ac susceptibility for $x=0.15$ sample.

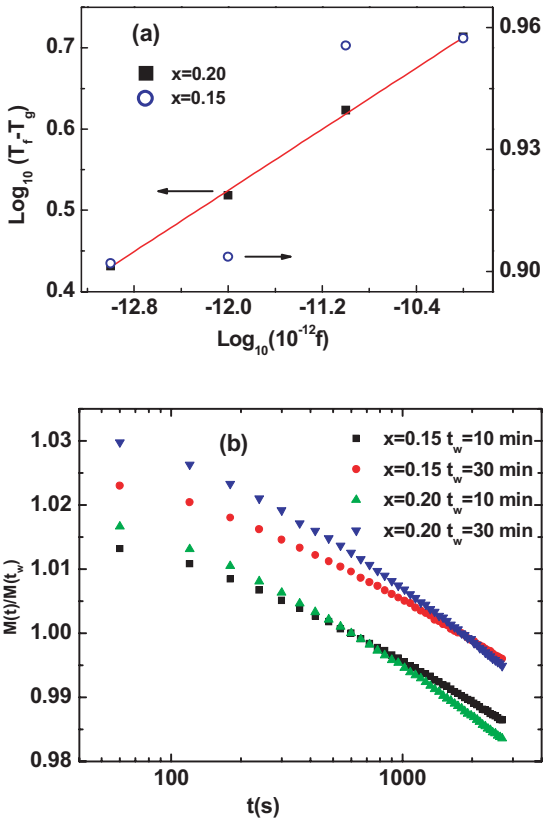

FIG. 8. (Color online) (a) The shifts of measured spin-glass ordering temperature T_f with frequency f of the ac magnetic field. Solid line indicates best-fitted line to the data with the critical slowing down power law relation ($\tau/\tau_0=\varepsilon^{-z\nu}$), described in the text. (b) Magnetic relaxation $[M(t)/M(t_w)]$ as a function of time t for $La_{0.7}Ca_{0.3}Mn_{1-x}Cd_xO_3$ sample with $x=0.15,0.20$. $M(t_w)$ is the observed value of magnetization at $t=t_w$.

neous for the sample and it remains in a mixed spin-glass and cluster-glass state.

A further investigation of the cluster-glass/spin-glass behavior is also done from the thermoremanent magnetization (TRM) measurements. The behavior of a spin glass below T_g is irreversible and complicated by the aging process, so it is imperative to employ a well-defined H-T procedure to obtain meaningful data. The sample was field cooled ($H=50$ Oe) down from 300 to 20 K and after certain waiting times ($t_w=10$ min and 30 min separately for each of the samples $x=0.15$ and 0.20), the field was reduced to zero and the corresponding decay of magnetization was recorded as a function of time. The results for the sample $x=0.15$ and 0.20 are shown in Fig. 8(b). The observed behavior is precisely the same as those of site-disordered spin glasses.[33] The longer the t_w, the slower the decay of the TRM. The system has become "stiffer" with time.

A comparison of the ac and dc magnetic properties show that although the low temperature bifurcation of the M-T data is prominent for all the higher Cd doped samples, the spin-glass phase is prominent and homogeneous only close to $x=0.20$. On the other hand, for $x=0.1$ and $x=0.15$, the sample remains in a mixed spin-glass and cluster-glass state. ac susceptibility data indicate [Figs. 7(a) and 7(b) insets and 8(a)] that the frequency shifts of the susceptibility curves are not uniform for the sample with $x=0.20$. The hysteresis curves also indicate that $x=0.10$ and $x=0.15$ samples contain weak AFM regions and the glassy behavior is not strong enough in this concentration range. Figure 9 represents a proposed transport and magnetic phase diagram for the $La_{0.7}Ca_{0.3}Mn_{1-x}CdO_3$ system showing effects of increasing disorder by substitution of Mn by Cd. From Fig. 9, seven phases—viz., paramagnetic insulator (PMI), paramagnetic metal (PMM), ferromagnetic metal (FMM), spin-glass insulator (SGI), cluster-glass insulator (CGI), cluster glass metal (CGM), and magnetic field-induced ferromagnetic (FIFM) (shaded region)—can be identified in the present system of our investigation

It is important to mention here that the effect of Cd doping at the La site has been investigated by Peña *et al.*[36] and others[37] in detail, showing quite different behavior from that of the corresponding Mn site doping system presented in this paper. The $La_{0.7}Ca_{0.3-x}Cd_xMnO_3$ system shows orthorhombic to rhombohedral transition[36,37] for $x=0.3$ and a suppression of double exchange is observed in this case. Interestingly, La site doping of Cd also induces a "spin-glass-like" metallic state in $La_{0.7}Ca_{0.3}MnO_3$ at low temperature,[38] whereas Mn site doping reduces the metallicity drastically and resulting in a low temperature insulating glassy state at $x=0.15$. The

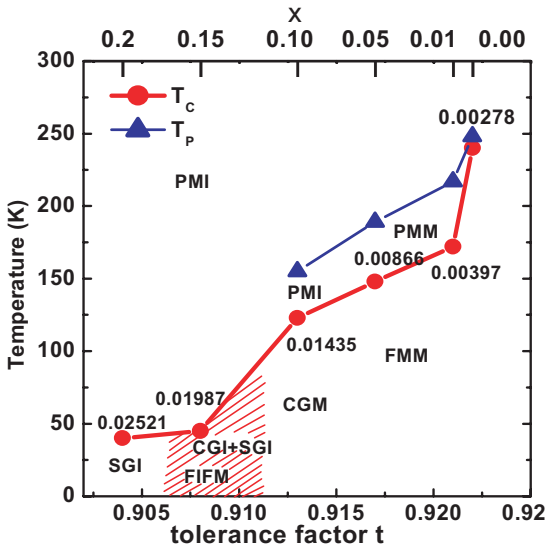

FIG. 9. (Color online) Electric and magnetic phase diagram for the $La_{0.7}Ca_{0.3}Mn_{1-x}Cd_xO_3$ ($0<x<0.3$) system. Seven phases [viz. paramagnetic insulator (PMI), paramagnetic metal (PMM), ferromagnetic metal (FMM), spin-glass insulator (SGI), cluster-glass insulator (CGI), cluster-glass metal (CGM), and magnetic field-induced ferromagnetic (FIFM)] (shaded region) can be identified. To see the effect of *B*-site cation disorder, the values of *B*-site ionic size variance "$\sigma^2=\Sigma x_i r_i^2-(\langle r_B\rangle)^2$" in $(Å)^2$ are indicated near the corresponding symbols. $\langle r_B\rangle$ is the average *B*-site ionic radius.

reason is that when Cd replaces Ca in $La_{0.7}Ca_{0.3}MnO_3$ system, the ratio Mn^{3+}/Mn^{4+} is unaltered, and the resultant changes are mainly due to structural distortion and grain boundary effects.[36] On the other hand, Mn site doping of Cd, in addition to structural changes, also alters the Mn^{3+}/Mn^{4+} ratio and hence the hole concentration of the $La_{0.7}Ca_{0.3}MnO_3$ system.

Finally, one more important issue to discuss is whether the spin/cluster-glass state depends on the tolerance factor/variance/size mismatch as strongly as the *A*-site doped systems do. We suggest that apart from the size mismatch due to the dopant ion, for the Mn site doped systems, 3*d* valency (hence the Mn^{4+}/Mn^{3+} ratio) also plays a key role in driving the spin-glass state. For comparison and completeness sake, the Mn site doped systems showing spin/cluster-glass properties are presented in Table IV. It is seen that the existence of the glassy phase is a general feature where Mn is substituted by closed shell $3d^0$ or ions such as Mg^{2+}, Al^{3+}, Sc^{3+}, Zn^{2+}, etc., irrespective of the fact that Al has a smaller ionic radius, whereas Mg, Sc, or Zn ions have a larger ionic radii than that of Mn^{3+}. Other 3*d* ions such as Cr and Fe also induce a spin-glass state. However, it appears that substitutions at the Mn site with ions having a stable electronic configuration, such as Al, Cd, Fe, Ga, Mg, Cu, etc.,[34] are more prone to the spin-glass state, whereas substitution with ions showing multiple valances, such as Co, Ni, Ru, Mo, etc., are not.[35] Substitutions by the later multivalent ions rather promote formation of magnetic clusters and not spin freezing in the system.

IV. CONCLUSION

Structural, magnetic, and transport properties of Cd doped $La_{0.7}Ca_{0.3}MnO_3$ samples prepared by sol-gel technique have been investigated. Cd concentration dependent PM to FM and PM to cluster/spin-glass behavior is exhibited by this system. The observed Curie temperature, spin-glass transi-

TABLE IV. Some of the Mn site doped systems showing spin/cluster glass properties.

Sample	x	Dopant ion radius (Å)[a]	Electronic configuration	Transition	Reference
$La_{0.7}Ca_{0.3}Mn_{1-x}Cd_xO_3$	0.15	Cd2+0.95	$Cd^{2+}=4d^{10}$	CS	This work
$La_{0.7}Ca_{0.3}Mn_{1-x}Cd_xO_3$	0.20	Cd2+0.95	$Cd^{2+}=4d^{10}$	SG	This work
$La_{0.7}Ca_{0.3}Mn_{1-x}Cr_xO_3$	0.05,0.1,0.3	$Cr^{3+}=0.615$	$Cr^{3+}=3d^3$	SG	15
		$Cr^{4+}=0.55$	$Cr^{4+}=3d^2$		
$La_{2/3}Ca_{1/3}Mn_{1-x}Cu_xO_3$	$x>0.05$	$Cu^{2+}=0.73$	$Cu^{2+}=3d^9$	CS	34
		$Cu^{3+}=0.54$	$Cu^{3+}=3d^8$		
$La_{2/3}Ca_{1/3}Mn_{1-x}Al_xO3$	$x=0.2$	$Al^{3+}=0.535$	$Al^{3+}=3d^0$	SG	15
$La_{0.7}Ca_{0.3}Mn_{1-x}Sc_xO_3$	$x=0.1$	$Sc^{3+}=0.745$	$Sc^{3+}=3p^6$	SG	15
$La_{2/3}Ca_{1/3}Mn_{1-x}Mg_xO_3$	$x=0.15,0.2$	$Mg^{2+}=0.72$	$Mg^{2+}=2p^6$	SG	34
$La_{0.67}Ca_{0.33}Mn_{1-x}Ga_xO_3$	$x=0.25$	$Ga^{3+}=0.620$	$Ga^{3+}=3d^{10}$	SG	15
$La_{0.7}Ca_{0.3}Mn_{1-x}Cu_xO_3$	$x=0.2$	$Cu^{2+}=0.73$	$Cu^{2+}=3d^{10}$	SG	27
$LaMn_{1-x}Mg_xO_3$	$x=0.3,0.4,0.5$	$Mg^{2+}=0.72$	$Mg^{2+}=3d^0$	SG	17
$La_{0.67}Ca_{0.33}Mn_{1-x}Fe_xO_3$	$x=0.1$	$Fe^{3+}=0.645$	$Fe^{3+}=3d^5$	SG	34
$La_{0.7}Pb_{0.3}Mn_{1-x}Ni_xO_3$	$x=0.3,0.4$	$Ni^{2+}=0.69$	$Ni^{2+}=3d^8$	CS	35
$La_{0.67}Sr_{0.33}Mn_{1-x}Ni_xO_3$	$x=0.2$	$Ni^{2+}=0.69$	$Ni^{2+}=3d^8$	CS	35
$La_{2/3}Ca_{1/3}Mn_{1-x}Ni_xO_3$	$x=0.1$	$Ni^{2+}=0.69$	$Ni^{2+}=3d^8$	SG	35

[a]Reference 21. CS=cluster/cluster glass state.

tion temperature, metal-insulator transition temperature, and MR values are very sensitive to even a very small amount of Cd doping. Besides the size mismatch of *A* and *B* site ions, the local strain effect due to introduction of larger 2+ ion for Mn ion also greatly effects the observed magnetic and transport properties. The increase in Mn-O distance and decrease in the nominal hole concentration due to addition of Cd in the system suppresses the double exchange and leads to a rise in resistivity and drop in T_C and T_p values. The nonavailability of Cd^{2+} for double exchange weakens the long-range ordering and promotes cluster formation and hence an enhancement of MR is observed. For $x \geqslant 0.1$, cluster/spin-glass transition was observed at low temperatures, which is confirmed and explained by considering interactions between the ferromagnetic and the antiferromagnetic clusters in the distorted system. The magnetic hysteresis loops for the samples with $x=0.15$ and 0.10 shows field-induced ferromagnetism. We can also conclude that Cd, in spite of being a larger sized cation (compared to Mn), is a very typical Group II*B* ion that substitutes Mn successfully, showing a wide range of magnetic phases and interesting properties such as a cluster-glass state, a spin-glass state, magnetization training effect, etc., depending on its concentration in the manganite system of the present investigation.

ACKNOWLEDGMENTS

Shilpi Karmakar and S. Taran acknowledge the Council of Scientific and Industrial Research (CSIR), Government of India, for financial support. These authors are also grateful to A. K. Majumdar, IIT Kanpur, for his valuable comments. This work was also partially supported by the National Science Council of Republic of China under Contract No. NSC94-2112-M110-010.

*Corresponding author. Email address: sspbkc@iacs.res.in

[1] S. Jin, T. H. Tiefel, M. McCormack, R. A. Fastnacht, R. Ramesh, and L. H. Chen, Science **264**, 413 (1994); R. von Helmolt, J. Wecker, B. Holzapfel, L. Schultz, and K. Samwer, Phys. Rev. Lett. **71**, 2331 (1993).

[2] Y. Tomioka, A. Asamitsu, Y. Moritomo, H. Kuwahara, and Y. Tokura, Phys. Rev. Lett. **74**, 5108 (1995); Z. Jirák, S. Krupička, Z. Šimša, M. Dlouhá, and S. Vratislav, J. Magn. Magn. Mater. **53**, 153 (1985); Z. Jirák, S. Krupička, V. Nekvasil, E. Pollert, G. Villeneuve, and F. Zounová, *ibid.* **15-18**, 519 (1980).

[3] A. Maignan, C. Martin, G. Van Tendeloo, M. Hervieu, and B. Raveau, Phys. Rev. B **60**, 15214 (1999).

[4] E. O. Wollan and W. C. Koehler, Phys. Rev. **100**, 545 (1955).

[5] C. Zener, Phys. Rev. **82**, 403 (1951).

[6] K. M. Krishnan and H. L. Ju, Phys. Rev. B **60**, 14793 (1999).

[7] N. Gayathri, A. K. Raychaudhuri, S. K. Tiwary, R. Gundakaram, A. Arulraj, and C. N. R. Rao, Phys. Rev. B **56**, 1345 (1997); S. L. Young, Y. C. Chen, H. Z. Chen, L. Horng, and J. F. Hsueh, J. Appl. Phys. **91**, 8915 (2002).

[8] J. Gutiérrez, A. Peña, J. M. Barandiarán, J. L. Pizarro, T. Hernández, L. Lezama, M. Insausti, and T. Rojo, Phys. Rev. B **61**, 9028 (2000).

[9] Y. Sun, W. Tong, X. Xu, and Y. Zhang, Appl. Phys. Lett. **78**, 643 (2001).

[10] B. M. Wu, B. Li, W. H. Zhen, M. Ausloos, Y. L. Du, J. F. Fagnard, and P. Vanderbemden, J. Appl. Phys. **97**, 103908 (2005).

[11] A. Machida, Y. Moritomo, K. Ohoyama, T. Katsufuji, and A. Nakamura, Phys. Rev. B **65**, 064435 (2002).

[12] Y. Moritomo, K. Murakami, H. Ishikawa, M. Hanawa, A. Nakamura, and K. Ohoyama, Phys. Rev. B **69**, 212407 (2004).

[13] J. Fan, L. Pi, W. Tong, S. Xu, J. Gao, C. Zha, and Yuheng Zhang, Phys. Rev. B **68**, 092407 (2003).

[14] V. P. S. Awana, E. Schmitt, E. Gmelin, A. Gupta, A. Sedky, A. V. Narlikar, O. F. de Lima, C. A. Cardoso, S. K. Malik, and W. B. Yelon, J. Appl. Phys. **87**, 5034 (2000); J. Blasco, J. García, J. M. de Teresa, M. R. Ibarra, J. Perez, P. A. Algarabel, C. Marquina, and C. Ritter, Phys. Rev. B **55**, 8905 (1997).

[15] J. Blasco, J. García, J. M. de Teresa, M. R. Ibarra, J. Perez, P. A. Algarabel, C. Marquina, and C. Ritter, Phys. Rev. B **55**, 8905 (1997); Bai-Mei Wu, Bo Li, Wei-Hua Zhen, M. Ausloos, Ying-Lei Du, J. F. Fagnard, and Ph. Vanderbemden, J. Appl. Phys. **97**, 103908 (2005); Yun-Hui Huang, Chun-Sheng Liao, Zhe-Ming Wang, Xiao-Hang Li, Chun-Hua Yan, Ji-Rong Sun, and Bao-Gen Shen, Phys. Rev. B **65**, 184423 (2002).

[16] S. M. Yusuf, M. Sahana, K. Dörr, U. K. Rößler, and K.-H. Müller, Phys. Rev. B **66**, 064414 (2002).

[17] J. M. De Teresa, M. R. Ibarra, J. García, J. Blasco, C. Ritter, P. A. Algarabel, C. Marquina, and A. del Moral, Phys. Rev. Lett. **76**, 3392 (1996).

[18] J. Blasco, J. García, G. Subías, and M. C. Sánchez, Phys. Rev. B **70**, 094426 (2004).

[19] Y. Moritomo, K. Murakami, H. Ishikawa, M. Hanawa, A. Nakamura, and K. Ohoyama, Phys. Rev. B **69**, 212407 (2004); A. M. L. Lopes, J. P. Araújo, A. M. Gomes, M. S. Reis, V. S. Amaral, and P. B. Tavares, J. Magn. Magn. Mater. **272**, 1767 (2004).

[20] C. Vázquez-Vázquez, M. C. Blanco, M. Arturo, M. A. López-Quintela, R. D. Sánchez, J. Rivas, and S. B. Oseroff, J. Mater. Chem. **8**, 991 (1998).

[21] P. M. Woodward, T. Vogt, D. E. Cox, A. Arulraj, C. N. R. Rao, P. Karen, and A. K. Cheetham, Chem. Mater. **10**, 3652 (1998); A. Barnabe, M. Hervieu, C. Martin, A. Maignan, and B. Raveau, J. Phys. Chem. Solids **62**, 1365 (2001).

[22] R. D. Shannon, Acta Crystallogr., Sect. A: Cryst. Phys., Diffr., Theor. Gen. Crystallogr. **32**, 751 (1976).

[23] M. Abbate, F. M. F. de Groot, J. C. Fuggle, A. Fujimori, O. Strebel, F. Lopez, M. Domke, G. Kaindl, G. A. Sawatzky, M. Takano, Y. Takeda, H. Eisaki, and S. Uchida, Phys. Rev. B **46**, 4511 (1992); E. Granado, R. R. Urbano, C. A. Pérez, C. Azimonte, J. W. Lynn, R. A. Souza, N. M. Souza-Neto, A. Y. Ramos, G. L. Bychkov, S. V. Shiryaev, and S. N. Barilo, *ibid.* **72**, 052406 (2005).

[24] K. Ghosh, S. B. Ogale, R. Ramesh, R. L. Greene, T. Venkatesan, K. M. Gapchup, R. Bathe, and S. I. Patil, Phys. Rev. B **59**, 533 (1999).

[25] D. Cao, F. Bridges, M. Anderson, A. P. Ramirez, M. Olapinski, M. A. Subramanian, C. H. Booth, and G. H. Kwei, Phys. Rev. B

64, 184409 (2001).

[26] N. F. Mott and E. A. Davies, *Electronic Processes in Noncrystalline Materials* (Oxford University Press, Oxford, 1971); A. Bannerjee, S. Pal, S. Bhattacharya, and B. K. Chaudhuri, J. Chem. Phys. **115**, 1550 (2001).

[27] X. Liu, X. Xu, and Y. Zhang, Phys. Rev. B **62**, 15112 (2000); L. Haupt, R. von Helmolt, U. Sondermann, K. Bärner, Y. Tang, E. R. Giessinger, R. Ladizinsky, and R. Braunstein, Phys. Lett. A **165**, 473 (1992).

[28] L. Pi, J. Cai, Q. Zhang, S. Tan, and Y. Zhang, Phys. Rev. B **71**, 134418 (2005).

[29] G. Cao, J. Zhang, S. Cao, C. Jing, and X. Shen, Phys. Rev. B **71**, 174414 (2005).

[30] S. C. Bhargava, H. P. Kunkel, S. Singh, S. K. Malik, D. D. Buddhikot, and A. H. Morrish, Phys. Rev. B **71**, 104419 (2005).

[31] J. Dho and N. H. Hur, Phys. Rev. B **67**, 214414 (2003).

[32] F. Wang, J. Zhang, Y. F. Chen, G. J. Wang, J. R. Sun, S. Y. Zhang, and B. G. Shen, Phys. Rev. B **69**, 094424 (2004); J. A. Mydosh, *Spin Glasses: An Experimental Introduction* (Taylor and Francis, London, 1993).

[33] A. S. Wills, V. Dupuis, E. Vincent, J. Hammann, and R. Calemczuk, Phys. Rev. B **62**, R9264 (2000).

[34] S. Tan, S. Yue, and Y. Zhang, Phys. Lett. A **319**, 530 (2003); K. Y. Wang, W. H. Song, J. M. Dai, S. L. Ye, S. G. Wang, J. Fang, J. L. Chen, B. J. Gao, J. J. Du, and Y. P. Sun, J. Appl. Phys. **90**, 6263 (2001).

[35] N. Gayathri, A. K. Raychaudhuri, S. K. Tiwary, R. Gundakaram, A. Arulraj, and C. N. R. Rao, Phys. Rev. B **56**, 1345 (1997); Z. H. Wang, B. G. Shen, N. Tang, J. W. Cai, T. H. Ji, J. G. Zhao, W. S. Zhan, G. C. Che, S. Y. Dai, and Dickon H. L. Ng, J. Appl. Phys. **85**, 5399 (1999); E. Granado, Q. Huang, J. W. Lynn, J. Gopalakrishnan, and K. Ramesha, Phys. Rev. B **70**, 214416 (2004); D. C. Kundaliya, R. Vij, R. G. Kulkarni, B. Varughese, A. K. Nigam, and S. K. Malik, J. Appl. Phys. **98**, 013905 (2005); S. Pal, E. Bose, B. K. Chaudhuri, H. D. Yang, S. Neeleshwar, and Y. Y. Chen, J. Magn. Magn. Mater. **293**, 872 (2005); M. Rubinstein, D. J. Gillespie, J. E. Snyder, and T. M. Tritt, Phys. Rev. B **56**, 5412 (1997); Z.-H. Wang, B.-G. Shen, N. Tang, J.-W. Cai, T.-H. Ji, J.-G. Zhao, W.-S. Zhan, G.-C. Che, S.-Y. Dai, and D. H. L. Ng, J. Appl. Phys. **85**, 5399 (1999).

[36] A. Peña, J. Gutiérrez, J. P. Chapman, J. M. Barandiarán, and T. Rojo, J. Magn. Magn. Mater. **242–245**, 679 (2002); A. Peña, J. Gutiérrez, J. M. Barandiarán, J. L. Pizarro, L. M. Rodríguez-Martínez, M. Insausti, and T. Rojo, J. Alloys Compd. **323-324**, 524 (2001); A. Peña, J. Gutiérrez, J. M. Barandiarán, J. P. Chapman, M. Insausti, and T. Rojo, J. Solid State Chem. **174**, 52 (2003).

[37] N. H. Luong, D. T. Hanh, N. Chau, N. D. Tho, and T. D. Hiep, J. Magn. Magn. Mater. **290&291**, 690 (2005); K. F. Wang, Q. Xiao, H. Yu, M. Zeng, M. F. Zhang, and J.-M. Liu, *ibid.* **285**, 130 (2005).

[38] G. Narsinga Rao, Saibal Roy, R. C. Yang, and J. W. Chen, J. Magn. Magn. Mater. **260**, 375 (2003).